



# Preparation of highly selective magnetic cobalt ion-imprinted polymer based on functionalized SBA-15 for removal $\text{Co}^{2+}$ from aqueous solutions

Zahra Adibmehr<sup>1</sup> · H. Faghihian<sup>2</sup>

Received: 7 January 2019 / Accepted: 30 December 2019 / Published online: 11 January 2020  
© Springer Nature Switzerland AG 2020

## Abstract

In this research, a novel magnetic cobalt ion imprinted adsorbent (Co(II)-MIIP) was synthesized by use of magnetic SBA-15 core-shell. It was functionalized by dithizone, and after identification by various techniques was used for removal of cobalt from aquatic systems. The uptake of cobalt proceeded very fast and achieved to equilibration within 5 min at which  $74 \text{ mg g}^{-1}$  of cobalt was adsorbed at  $\text{pH} = 8$  with adsorbent dose of 0.15 g. The ion imprinted sorbent exhibited good selectivity towards cobalt ions. Separation and recovery of the used sorbent was carried out respectively by use of magnetic field and by use of  $\text{HNO}_3$  (0.1 M), and 85% of the initial capacity was obtained after seven 7 regeneration cycles. Different isotherm models, and error analysis were used to evaluate the experimental data. Thermodynamic, and kinetic evaluations showed that sorption process was endothermic, and described by second order kinetic model ( $R^2 > 0.99$ ). The equilibrium was established within five min.

**Keywords** Magnetic sorbent · Co(II)-MIIP: Mesoporous silica · Functionalization · Cobalt; dithizone

## Introduction

Cobalt which is widely employed in different industries causes a variety of health problems in human beings [1–4], thus its removal from aquatic systems is inevitable [5–7]. Many techniques have been considered for removal of cobalt, such as precipitation [8], use of ion exchangers [9], coagulation [10], biological methods [11], osmosis techniques [12], and sorption [13]. Adsorption technique, due to its high efficiency, flexibility, and regeneration capability is the most frequently used method. The basic requirement of the method is preparation of an adsorbent with acceptable selectivity and capacity, particularly when the matrix of the target samples is complicated. To prepare an

adsorbent with above properties, imprinted sorbents can be considered. Ion-imprinted polymers (IIP) are versatile sorbents comprising of target ions encapsulated in polymers network, and after removal of the ions, the cavities left inside the network are interestingly prone to selectively adsorb the target cation from the solutions with complicated matrix [14–16]. Ion imprinting process involves three distinct steps including complexation of template (ion) with a particular ligand, polymerization of the produced complex, and removal of the ion after co-polymerization [17, 18]. Mesoporous materials due to their particular structural feasibility and abundant Si-OH active bonds on the surface are excellent candidate as solid supports for many applications such as synthesis of ion imprinted sorbents [19, 20]. Among them, SBA-15 has two-dimensional structure with large surface area, high pore volume, uniform and thick pores with large diameters, and excellent hydrothermal stability [21, 22].

In the present research, a novel cobalt ion-imprinted polymer was synthesized on the basis of magnetic SBA-15 treated with chloropropyltriethoxysilane, and dimethacrylate as cross linker. The sorbent was employed for uptake of  $\text{Co}^{2+}$  from aquatic systems under different experimental conditions.

**Electronic supplementary material** The online version of this article (<https://doi.org/10.1007/s40201-019-00439-x>) contains supplementary material, which is available to authorized users.

✉ H. Faghihian  
faghihian@iaush.ac.ir

<sup>1</sup> Department of Chemistry, Firoozabad Branch, Islamic Azad University, P.O. Box 74715-117, Firoozabad, Fars, Iran

<sup>2</sup> Naghshejahan Higher Education Institute, Isfahan, Iran

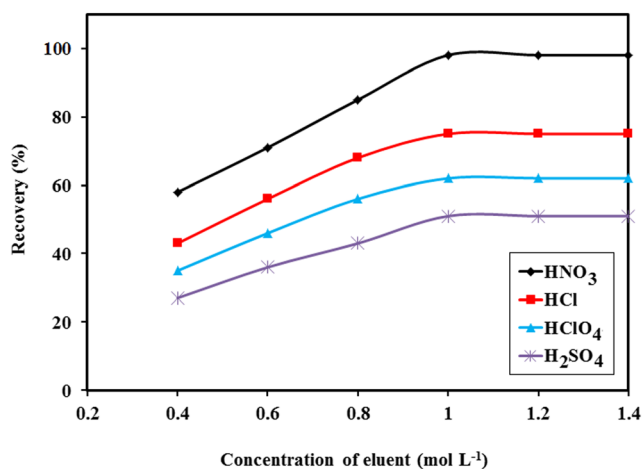


**Fig. 1** Effect of type and concentration of acid on magnetic ion imprinted polymer

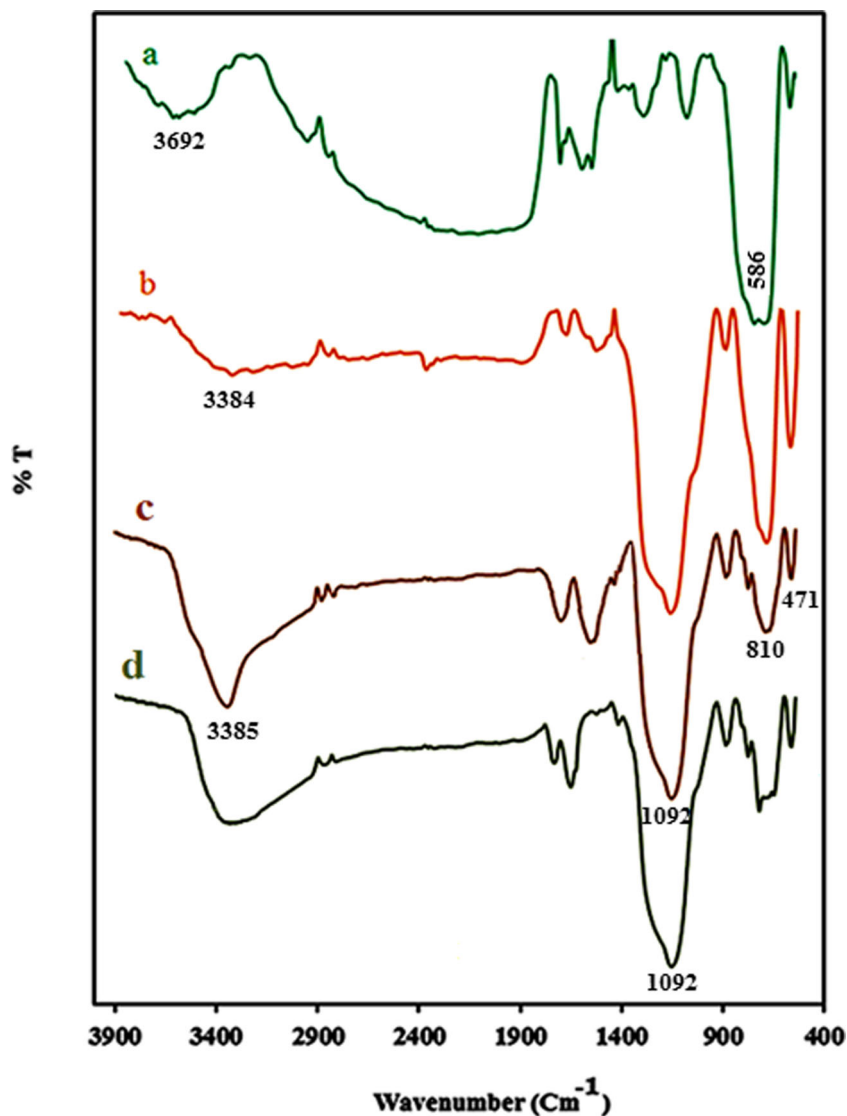
## Experimental

### Chemicals and apparatus

Fe (III) chloride, Fe (II) chloride, sodium hydroxide, nitric acid, sulfuric acid, HCl, HClO<sub>4</sub>, CH<sub>3</sub>OH, and Co(NO<sub>3</sub>)<sub>2</sub>, NH<sub>4</sub>F, C<sub>2</sub>H<sub>5</sub>OH, and were purchased from Merck Company. Pluronic (P123, PEO<sub>20</sub>PPO<sub>70</sub>PEO<sub>20</sub>), chloropropyltriethoxysilane (CPTES), methacrylic acid (MAA) and 2,2-azobisisobutyronitrile (AIBN) were obtained from Sigma Aldrich Company, and ethylene glycol dimethacrylate (EGDMA) from Fluka (Bunche, Switzerland).

FT-IR spectra were taken by use of a Perkin Elmer model 65 instrument from 400 to 4000 cm<sup>-1</sup>. A Micromeritics BET instrument, model ASAP2020 (USA) was used to measure the

**Fig. 2** FT- IR Spectra (a) Fe<sub>3</sub>O<sub>4</sub>, (b) SiO<sub>2</sub>@Fe<sub>3</sub>O<sub>4</sub>, (c) Co(II)-MIP, and (d) Leached Co(II)-MIP



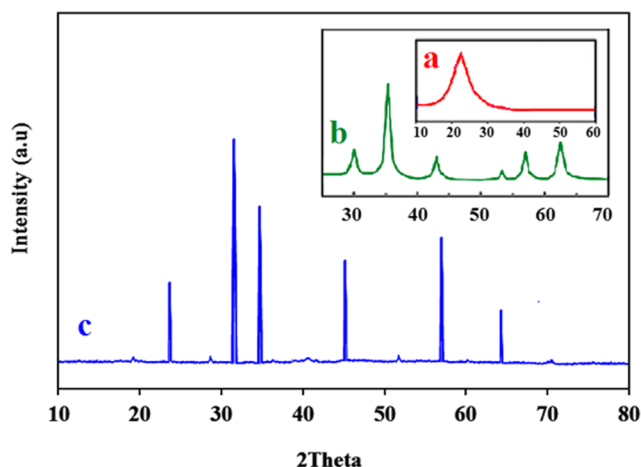


Fig. 3 XRD Spectra (a) SBA-15, (b) Fe<sub>3</sub>O<sub>4</sub>, and (c) Co(II)-MIIP

surface area of sorbents. A X\Pert Pro X-ray diffractometer (Philips, Netherlands) was employed to prepare the XRD pattern of the samples. The SEM images were taken using a FE-SEM TESCAN scanning electron microscope. VSM measurements were performed by use a LDJ Electronics Inc., Model 9600 magnetometer, and thermal curves were prepared by a Netzsch STA 409 device. Cobalt concentration was determined by a Perkin Elmer model A., Analyst 300 spectrometer at 240.7 nm.

### Synthesis of magnetic ion-imprinted polymer

The procedure described by Wang with little modification was used to synthesize the magnetic SBA-15 core shell (Fe<sub>3</sub>O<sub>4</sub>@SBA-15) [23]. A solution containing 0.04 mol of FeCl<sub>3</sub>.6H<sub>2</sub>O and 0.02 mol of FeCl<sub>2</sub>.4H<sub>2</sub>O dissolved in 50 mL of HCl (0.5 M) was prepared and heated to 80 °C. Sodium hydroxide (0.1 M) was drop wise added with vigorous stirring and under nitrogen atmosphere until Fe<sub>3</sub>O<sub>4</sub> formation was completed. The particles were collected by a magnet, rinsed with water, and vacuum dried

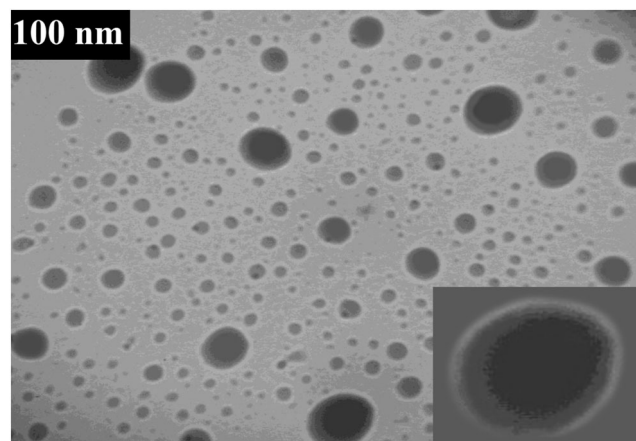


Fig. 4 TEM image of Co(II)-MIIP

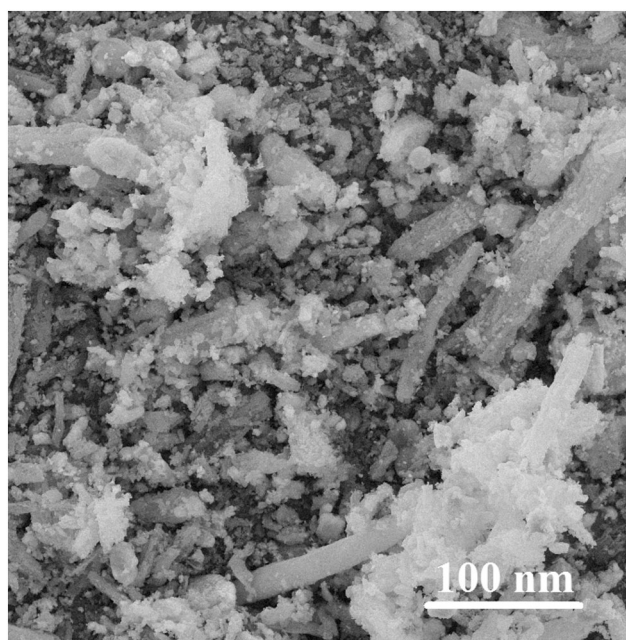


Fig. 5 SEM image of Co(II)-MIIP

at 60 °C. A mixture containing 1.0 g of the dried powder, 80 mL of C<sub>2</sub>H<sub>5</sub>OH, 20 mL water and 2 mL NH<sub>4</sub>OH (28 W%) was prepared, and was ultrasonicated for 10 min. 1 mL of tetraorthosilicate (TEOS) was then gradually added while vigorously shaking until magnetic particles were formed. The particles were collected by a magnet, rinsed respectively by H<sub>2</sub>O and C<sub>2</sub>H<sub>5</sub>OH, and vacuum dried at 55 °C. 4.0 g of P123 was added into 100 mL of HCl (0.1 M) solution containing 0.046 g of NH<sub>4</sub>F, shaken until proper homogenization, 9.0 mL of tetraorthosilicate was drop wise added, and the mixture was shaken till core-shell (Fe<sub>3</sub>O<sub>4</sub>@SBA-15) was pro-

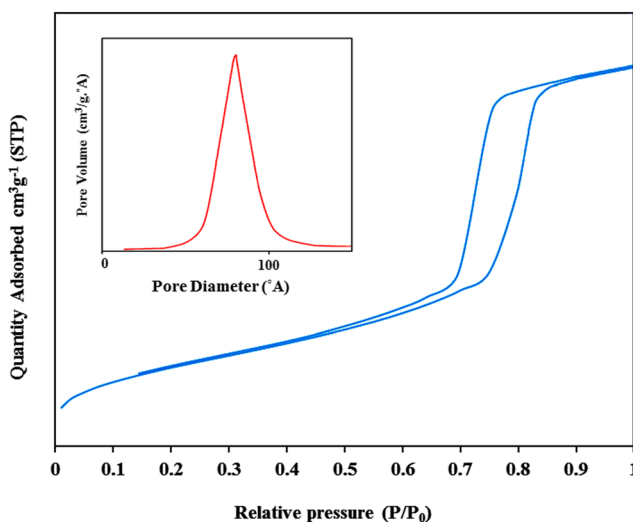


Fig. 6 N<sub>2</sub> adsorption-desorption isotherms of Co(II)-MIIP

**Table 1** Surface area, Pore volume and pore diameter of Co(II)-MIIP sample

| Adsorbent                              | BET surface area (m <sup>2</sup> g <sup>-1</sup> ) | Pore volume (cm <sup>3</sup> g <sup>-1</sup> ) | Pore diameter (°A) | Ref.       |
|--|--|--|--------------------|------------|
| Fe <sub>3</sub> O <sub>4</sub> @SBA-15 | 784.8  | 1.83   | 79                 | [23]       |
| Co(II)-MIIP                            | 254.0  | 0.41   | 52                 | This study |

duced. The product was separated and heat treated at 560 °C for 8 h [24].

Functionalization of magnetized SBA-15 (Fe<sub>3</sub>O<sub>4</sub>@SBA-15) was performed as follows:

50 mL of dry toluene was added to 5.0 g of core-shell, shaken until proper homogenization, after adding 20.76 mmol of CPTES, the mixture was refluxed at 82 °C for 20 h. Chlorinated core shell (Fe<sub>3</sub>O<sub>4</sub>@SBA-15-Cl) was removed, washed with water and dried at 120 °C under vacuum [25]. 25 mL of acetonitrile was added to 2.0 g of Fe<sub>3</sub>O<sub>4</sub>@SBA-15-Cl, shaken for 60 min, and after adding 0.25 g of dithizone (DZ) the mixture was refluxed at 85 °C for 8 h. The functionalized material (Fe<sub>3</sub>O<sub>4</sub>@SBA-15-DZ) was filtered, washed with C<sub>2</sub>H<sub>5</sub>OH and dried at 50 °C under vacuum. Finally, the Co(II)-MIIP adsorbent was prepared by surface imprinting of the Fe<sub>3</sub>O<sub>4</sub>@SBA-15-DZ as follows:

A suspension prepared by adding of 50 mg Fe<sub>3</sub>O<sub>4</sub>@SBA-15-DZ into 60 mL of acetonitrile was added to solution contained 0.2 mmol of Co(NO<sub>3</sub>)<sub>2</sub>·6H<sub>2</sub>O, 1.0 mmol of MAA, 3 mmol of EGDMA and 40 mg of AIBN, and then was agitated at 65 °C for 20 h. The produced (Co(II)-MIIP) was removed, washed with methanol and distilled water repeatedly and dried at 30 °C. Through the same procedure, and without adding cobalt nitrate solution, non-imprinted polymer was synthesized.

## Sorption performance of co(II)-MIIP

### Elution of cobalt

The eluent used for removing of cation from ion-imprinted sorbent should properly wash out the cation without affecting

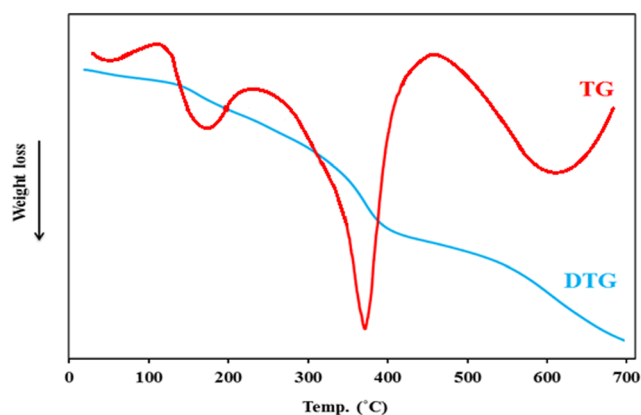


**Fig. 7** TG and DTG curves of Co(II)-MIIP

the ligand and polymer structure. To select an adequate eluent, the Co(II)-MIIP sorbent was eluted with various acids such as; nitric, sulfuric, perchloric and hydrochloric acids with different concentrations. The results indicated that with HNO<sub>3</sub> (1 M) the optimized recovery percentage was obtained (Fig. 1).

### Removal of cobalt

The removal efficiency of the ion imprinted sorbent was optimized by studying the effect of different variables through following experiments:

Into 25 mL of cobalt solution (200–1400 mg L<sup>-1</sup>) a predetermined amount of adsorbent (0.05–0.2 g) was added, the pH of the solution was adjusted to (2–10), and the mixture was agitated for 20 min at particular temperature (25–55 °C). The sorbent was removed, and the concentration of cobalt in the filtrate was determined by the calibration curve constructed in the concentration ranges of 5–30 mg L<sup>-1</sup>. The uptake of cobalt, was measured by eq. (1):

$$q = (C_i - C_f) \times (V/m) \quad (1)$$

$C_i$  and  $C_f$  are Co<sup>2+</sup> initial and final concentration respectively (mg L<sup>-1</sup>),  $m$  is sorbent weight (g), and  $V$  is solution volume (L). To evaluate the effect of different variables, a

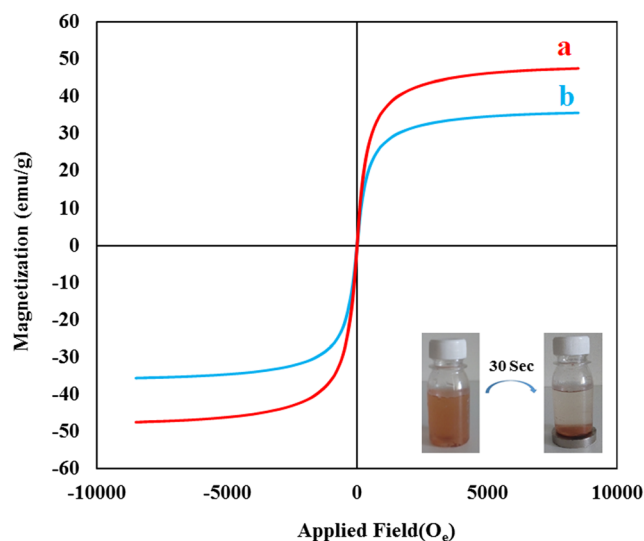


**Fig. 8** Magnetic hysteresis loops of (a) Fe<sub>3</sub>O<sub>4</sub>@SBA-15-Cl, and (b) Co(II)-MIIP

**Table 2** Compared magnetization properties Co(II)-MIIP with other adsorbents

| Adsorbent   | Monomer  | emu/g | Ref.       |
|-------------|--|-------|------------|
| Pb(II)-MIIP | 2-vinylpyridine                                      | 8.3   | [32]       |
| Pb(II)-MIIP | 4-(vinylamino)pyridine-2,6-dicarboxylic acid (VPyDC) | 1.96  | [33]       |
| Pb(II)-MIIP | 4-vinylpyridine (4VP)                                | 13.5  | [34]       |
| Pb(II)-MIIP | methacrylic acid, salicylaldehyde                    | 1.96  | [35]       |
| Cd(II)-MIIP | methacrylic acid                                     | 4.88  | [36]       |
| Cd(II)-MIIP | dithizone  | 44.6  | [37]       |
| Cu(II)-MIIP | 3-aminopropyltriethoxysilane (APTES)                 | 50.6  | [38]       |
| Co(II)-MIIP | dithizone  | 51    | This study |

series of experiments was carried out by changing the appropriate variable and keeping the rest constant.

## Discussion of the results

### Characterization of adsorbent

In FT-IR spectra of Fe<sub>3</sub>O<sub>4</sub> (Fig. 2a), the broad band of O-H vibration and the absorption band of Fe-O stretching were observed at 3692, and at 586 cm<sup>-1</sup> respectively.

In FT-IR spectra of SiO<sub>2</sub>@Fe<sub>3</sub>O<sub>4</sub> (Fig. 2b), the broad bands belonged to O-H vibration and Fe-O stretching were observed at 3384 cm<sup>-1</sup> at 586 cm<sup>-1</sup> respectively, and the Si-O-Si band was appeared at 1090 cm<sup>-1</sup>.

FT-IR spectrum of Co(II)-MIIP exhibited in fig. 2c, showed the absorption band of O-H of silane groups and water molecules at 3385 Cm<sup>-1</sup>. Symmetric and asymmetric stretching and bending of Si-O-Si were respectively appeared at 1092, 810 and 471 Cm<sup>-1</sup> regions [26]. The band appeared at 2932 Cm<sup>-1</sup> was related to vibration of C-H bond. The band related to C-Cl bond was

disappeared after reaction between SBA-15-Cl with NH of dithizone. The C-H, and C=S stretching of DZ were observed at 2984 and at 1612 Cm<sup>-1</sup> respectively. After polymerization, the peaks belonged to C=O and C-H bonds were appeared around 1700 and 2830 cm<sup>-1</sup> respectively, and the peak related to Fe-O was observed at 586 Cm<sup>-1</sup> indicating formation of iron-oxygen bonds in Co(II)-MIIP sorbent [24].

FT-IR spectrum of leached Co(II)-MIIP is exhibited in Fig. 2d. After leaching of Co(II), the bands related to C=S of DZ, OH of MAA, and N-H of DZ remained unchanged indicating that elution of cobalt by acid did not change the structure of sorbent [27].

In the XRD of SBA-15, the characteristic diffraction band of hexagonal SBA-15 were appeared at 20–30° (Fig. 3a) [28]. In the XRD pattern of Fe<sub>3</sub>O<sub>4</sub>, The diffraction lines of magnetite cubic spinel were observed at 2θ of 30.4, 35.6, 43.3, 57.3, and 62.8 (Fig. 3b) [23]. The position of these line was slightly changed in the XRD pattern of Co(II)-MIIP, and appeared respectively at 2θ = 31, 36, 43, 60, and 63 indicating that Fe<sub>3</sub>O<sub>4</sub> maintained its initial structure after combination with SBA-15 (Fig. 3c).

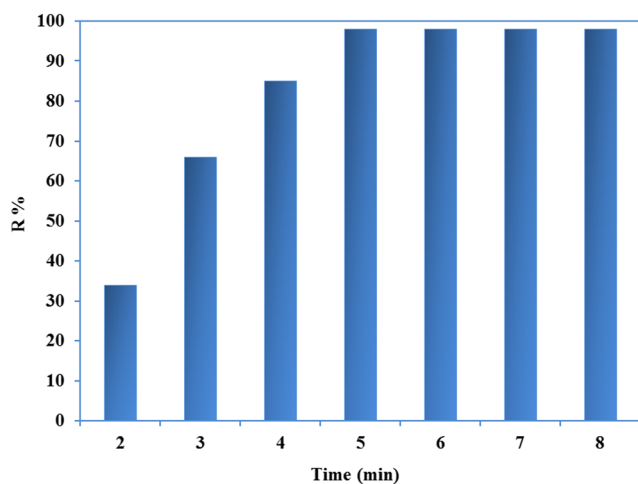


**Fig. 9** Effect of contacting time on the sorption process

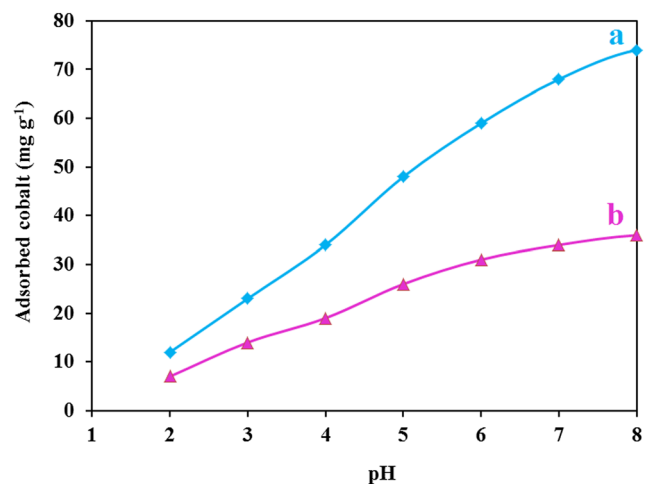


**Fig. 10** Effect of pH on the removal of the cobalt cation by Co(II)-MIIP (a) Co(II)-MIIP, (b) Magnetic non ion imprinted polymer

**Table 3** Compared pH and adsorption capacity Co(II)-MIIP with other adsorbents

| Adsorbent   | Monomer  | pH | Adsorption capacity (mg g <sup>-1</sup> ) | Ref.       |
|-------------|--|----|---|------------|
| Co(II)-MIIP | 1-vinylimidazole                                     | 7  | 23.09                                     | [39]       |
| Co(II)-MIIP | polyethyleneimine (PEI)                              | 5  | 39.26                                     | [40]       |
| Co(II)-MIIP | 3-(2-aminoethylamino) propyltrimethoxysilane (AAPTS) | 8  | 35.21                                     | [41]       |
| Co(II)-MIIP | dithizone  | 6  | 74.00                                     | This study |

In the EDAX spectrum of Co(II)-MIIP the presence of C, N, O, Si, Fe, and Co was clearly observed (Fig. 1S). Careful investigation of map of elements (Fig. 2S), revealed that they were uniformly distributed on the adsorbent surface which was helpful for easy access of the ingoing cations to the adsorption sites.

TEM image of Fe<sub>3</sub>O<sub>4</sub>@SBA-15 showed that magnetic core-shell has been formed. The magnetic particles were situated as spherical dark core of the core-shell which were surrounded by SiO<sub>2</sub> particles (Fig. 4).

The SEM image of Co(II)-MIIP is represented in Fig. 5. Formation of rectangular beads of SBA-15 crystals was observed. The average particle diameter of Co(II)-MIIP estimated by Image-j software was 77 nm.

The specific surface area, pore volume and pore distribution was studied by nitrogen adsorption-desorption isotherms, and by use of Brunauer–Emmett–Teller (BET), and Barrett–Joyner–Halenda (BJH) equation. The specific surface area, pore volume and pore diameter of Fe<sub>3</sub>O<sub>4</sub>@SBA-15 was considerably decreased after polymerization because the channels and voids were partially engaged (Fig. 6), and Table 1. However, the surface area of the sorbent was sufficiently high to adsorb considerable amount of cobalt.

TG-DTG of sorbent was prepared in N<sub>2</sub> from 35 to 720 °C (Fig. 7). The peak appeared between 100 and 200 °C belonged

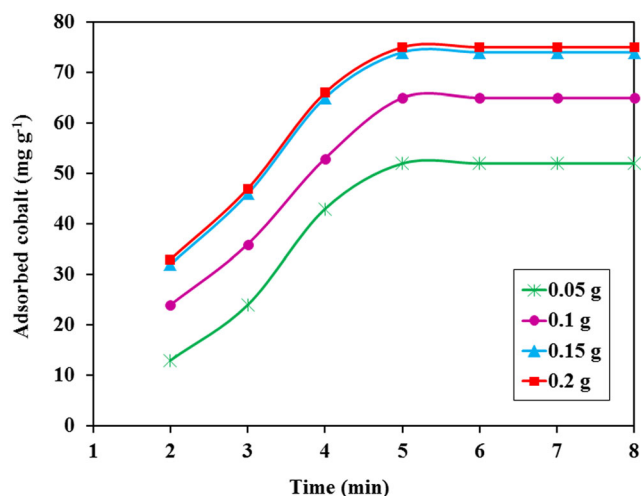
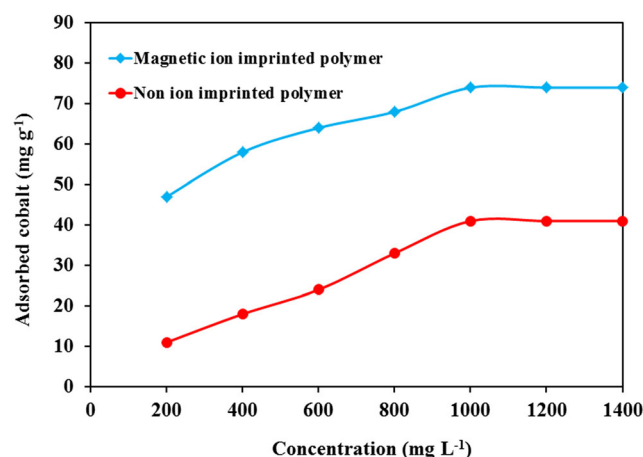
to elimination of water molecules, and that appeared between 350 and 400 °C was attributed to the ligand eliminated from the surface of adsorbent [29]. The weight loss appeared at 600 °C belonged to conversion of Fe<sub>3</sub>O<sub>4</sub> to  $\gamma$ -Fe<sub>2</sub>O<sub>3</sub> or FeO [30, 31].

The magnetization saturation of Fe<sub>3</sub>O<sub>4</sub>@SBA-15-Cl, and Co(II)-MIIP was 51 and 40 emu/g respectively (Fig. 8). Lower magnetization of Co(II)-MIIP compared to Fe<sub>3</sub>O<sub>4</sub>@SBA-15-Cl was related to the polymerization process, in which the surface of magnetized sorbent was shielded by the polymer molecules. However, as indicated in Table 2, the saturation magnetization of adsorbent was higher than the previously studied magnetic adsorbents. However, the magnetization of adsorbent affiliated its separation by the external magnetic field [32–38].

## Optimization of effecting variables

### Shaking time

By increasing of shaking time, the uptake of cobalt was increased, and achieved to its maximal level after 5.0 min (Fig. 9). The fast kinetic of adsorption was very advantageous for uptake of the studied cation.

**Fig. 11** Effect of adsorbent dose on the percentage removal of cobalt ions**Fig. 12** Effect of cobalt initial concentration on adsorption capacity of Co(II)-MIIP

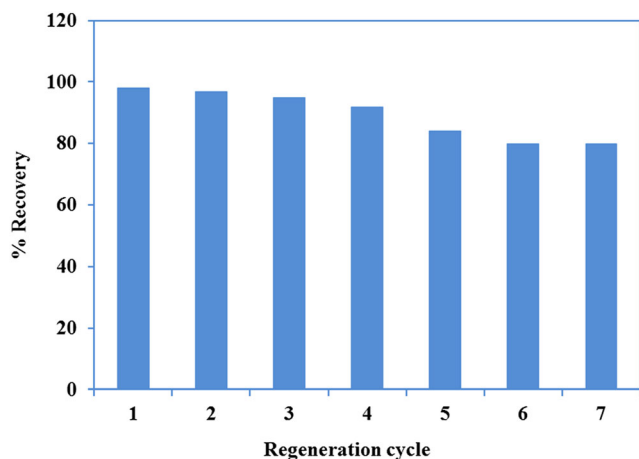


Fig. 13 Regeneration of adsorbent

**pH of solution**

Solution pH can strongly affect the uptake of cations because it may change the surface charge of the adsorbent, the  $H_3O^+$  concentration, and cationic form of the metal ion. Additionally, at higher pHs the cation may precipitate. To investigate the pH effect on the uptake of cobalt, following experiment performed in pH range of (2–10):

A mixture containing 0.1 g of sorbent added into 25 mL of cobalt solution ( $1000\text{ mg L}^{-1}$ ), was gently shaken for 20 min, at an adjusted pH. Then sorbent was removed, and cobalt concentration was determined (Fig. 10). The adsorption capacity increased as the pH increased, achieved to optimum capacity at  $\text{pH} = 8$ , and then became constant. At low pHs, the ligands attached to the adsorbent were protonated, and the formation of complex between the sorbents and cobalt ions was not favored. Additionally, the repulsive force between protonated sites and the positively charged cobalt reduced the uptake of the cation. As the pH was increased, free electron pair of ligand reduced the repulsion force, and more cation were reacted with the ligands. The pHs above 8.0 were not examined because cobalt ions were precipitated as  $\text{Co}(\text{OH})_2$  [38]. Adsorption capacity of the non-ion imprinted sample was significantly smaller than ion imprinted sorbent. To have more clear image of the pH effect,  $\text{PHpzc}$  of the sorbent was determined (Fig. 3S). The surface had no charge at  $\text{pH} = 7.3$ . At lower pH, a repulsion force between cobalt ions and the sorbent was created which limited the uptake of cation. At  $\text{pH} > 7.3$ , the negative surface attracted  $\text{Co}^{+2}$ , and

the maximal level of uptake was achieved at at  $\text{pH} = 8$ . It is assumed that the optimized pH for each individual ion imprinted sorbents polymers depends on to the ligand type, therefore it is different for various sorbents (Table 3) [39–41].

**Sorbent dosage**

To evaluate the effect of adsorbent dose on the uptake of cobalt, several adsorption experiments were carried out with different amount of  $\text{Co}(\text{II})\text{-MIIP}$  (0.05–0.2 g) while the other experimental variables were kept constant (Fig. 11). The uptake of cobalt was increased and achieved to its maximum level with dosage of 0.15 g. At constant concentrations of cation, the increase of sorbent dose, generate more sorption sites which increased the capacity. The increase was continued until the adsorption sites and cobalt ions were in balance, then the adsorption process remained constant.

**Cobalt concentration**

Under optimized conditions,  $\text{Co}^{2+}$  concentration was changed from 200 to  $1400\text{ mg L}^{-1}$ , and the uptake of cobalt was measured (Fig. 12). At higher concentration, the diffusion of ingoing cation to the adsorption sites were facilitated, so that the optimized value was obtained at  $1000\text{ mg L}^{-1}$ , and with further increase of concentration, the absorption capacity remained constant. Similar behavior has been reported for different adsorbents.

In Yan et al. studied the effect of cobalt concentration on the uptake by polyethyleneamine and reported that the maximal adsorption capacity was obtained at  $100\text{ mg L}^{-1}$  [40]. Khoddami et al. used magnetic ion-imprinted polymer for uptake of cobalt and concluded that maximal uptake was obtained at certain concentration, and at higher concentration the uptake remained constant because the sites were fully engaged [41].

**Regeneration of the adsorbent**

The recovery of adsorbent was performed by elution of cobalt from the sorbent by 25 mL of  $\text{HNO}_3$  (1 M), and using the regenerated sorbent for adsorption process at optimized conditions. As discussed in section 3.2.1, the sorption-desorption steps were kinetically fast, therefore employment of sorbent

**Table 4** Compared recovery efficiency  $\text{Co}(\text{II})\text{-MIIP}$  with other adsorbents

| Adsorbent                          | Monomer  | Cycle | R % | Ref.       |
|------------------------------------|--|-------|-----|------------|
| $\text{Co}(\text{II})\text{-MIIP}$ | 1-vinylimidazole                                     | 4     | 81% | [39]       |
| $\text{Co}(\text{II})\text{-MIIP}$ | polyethyleneimine (PEI)                              | 6     | 95% | [40]       |
| $\text{Co}(\text{II})\text{-MIIP}$ | 3-(2-aminoethylamino) propyltrimethoxysilane (AAPTS) | 7     | 95% | [41]       |
| $\text{Co}(\text{II})\text{-MIIP}$ | dithizone  | 7     | 85% | This study |

**Table 5** Selectivity of MIIP in the presence of competing cations (Cobalt Conc. = 1000 mg L<sup>-1</sup>)

| Interference ion     | Tolerable concentration ratio X <sup>a</sup> /Co | MIIP R (%) | NIIP R (%) |
|----------------------|--|------------|------------|
| Without interference | –  | 98.0       | 46.0       |
| Na <sup>+</sup>      | 10   | 94.2       | 41.3       |
| K <sup>+</sup>       | 10   | 93.6       | 41.6       |
| Ca <sup>2+</sup>     | 10   | 93.4       | 42.6       |
| Mg <sup>2+</sup>     | 10   | 92.9       | 42.4       |
| Ni <sup>2+</sup>     | 10   | 89.6       | 40.6       |
| Zn <sup>2+</sup>     | 10   | 89.4       | 40.5       |
| Fe <sup>2+</sup>     | 10   | 90.7       | 39.9       |
| Mn <sup>2+</sup>     | 10   | 91.2       | 39.3       |
| Cu <sup>2+</sup>     | 5  | 92.5       | 38.9       |
| Cd <sup>2+</sup>     | 5  | 92.8       | 39.8       |
| Pb <sup>2+</sup>     | 5  | 92.8       | 40.2       |
| Hg <sup>2+</sup>     | 5  | 91.9       | 38.6       |

<sup>a</sup> Concentration of various ions

for consecutive uptake of cobalt was quite feasible. The regeneration cycles was repeated for 7 successive cycles (Fig. 13). The regenerated capacity was respectively 98% after the first and 85% after the last step. For comparison, the regeneration capability of similar sorbent are given in Table 4.

**Table 6** Langmuir, Freundlich and Redlich-Peterson isotherm parameters

| Isotherm         | Parameter        | Value    |
|------------------|------------------|----------|
| Langmuir         | K <sub>L</sub>   | 5.88 E-3 |
|                  | q <sub>m</sub>   | 84.03    |
|                  | R <sup>2</sup>   | 0.9978   |
|                  | SSE              | 13.08    |
|                  | ARE              | 0.0199   |
| Freundlich       | K <sub>F</sub>   | 13.31    |
|                  | n                | 4.11     |
|                  | R <sup>2</sup>   | 0.9728   |
|                  | SSE              | 22.88    |
|                  | ARE              | 0.022    |
| Redlich-Peterson | A                | 0.6      |
|                  | B                | 0.0098   |
|                  | g                | 0.96     |
|                  | R <sup>2</sup>   | 0.9988   |
|                  | SSE              | 11.31    |
|                  | ARE              | 0.015    |
| Sips             | K <sub>S</sub>   | 6.53 E-3 |
|                  | Q <sub>max</sub> | 81.97    |
|                  | m                | 1        |
|                  | R <sup>2</sup>   | 0.9858   |
|                  | SSE              | 14.52    |
|                  | ARE              | 0.018    |

Depend on the nature of ion imprinted sorbents and their ligands, the regenerated capacity was between 81 to 95%.

### Selectivity of adsorbent

To study the selectivity of the ion imprinted sorbent, the removal of cobalt was measured at optimized conditions while the concentration of co-existing ions; Na<sup>+</sup>, K<sup>+</sup>, Ca<sup>2+</sup>, Mg<sup>2+</sup>, Ni<sup>2+</sup>, Zn<sup>2+</sup>, Fe<sup>2+</sup>, Mn<sup>2+</sup>, Pb<sup>2+</sup>, Cd<sup>2+</sup>, Cu<sup>2+</sup> and Hg<sup>2+</sup> was slowly increased. To evaluate the interfering effect of the cations, the tolerance limit was considered as the highest concentration of the ions causing less than 5% change on the uptake of Co<sup>2+</sup> (Table 5). For Na<sup>+</sup>, K<sup>+</sup>, Ca<sup>2+</sup>, Mg<sup>2+</sup>, Ni<sup>2+</sup>, Zn<sup>2+</sup>, Fe<sup>2+</sup> and Mn<sup>2+</sup>, the sorbent selectivity at ratio of 10:1 was acceptable, while its selectivity in the presence of for Cu<sup>2+</sup>, Cd<sup>2+</sup>, Pb<sup>2+</sup> and Hg<sup>2+</sup> at ratio concentration of 5:1 was acceptable.

From the results it can be concluded that sorbent was not much affected by alkaline and alkaline earth metals, therefore this method can be used for uptake of cobalt from real samples in which the concentration of co-existing cations is high. The high selectivity of adsorbent toward cobalt ions is attributed to high affinity of cobalt as a transition element to form a stable complex with the ligand, and to ion imprinting nature of the sorbent. Non imprinted sorbent showed no selectivity for cobalt under identical experimental conditions.

**Table 7** Kinetic parameters of cobalt ions adsorption by the Co(II)-MIIP adsorbent

| Adsorbent   | Pseudo-first-order |                |                | Pseudo-second-order |                |                |
|-------------|--------------------|----------------|----------------|---------------------|----------------|----------------|
|             | q <sub>e</sub>     | K <sub>1</sub> | R <sup>2</sup> | q <sub>e</sub>      | K <sub>2</sub> | R <sup>2</sup> |
| Co(II)-MIIP | 80.9               | 9.67 E-3       | 0.9796         | 105.26              | 6.77 E-5       | 0.9964         |



**Table 8** Thermodynamic parameters of cobalt ions adsorption by Co(II)-MIIP

| Adsorbent   | T(°K) | ΔG° (kJ mol <sup>-1</sup> ) | ΔH° (kJ mol <sup>-1</sup> ) | ΔS° (J mol <sup>-1</sup> ) | R <sup>2</sup> |
|-------------|-------|-----------------------------|-----------------------------|----------------------------|----------------|
| Co(II)-MIIP | 298   | 6.54                        | 1.08                        | -18.04                     | 0.9995         |

### Sorption isotherms evaluation

To compare the performance of different sorbents and to determine the optimal conditions for adsorption, the sorption isotherms which represent the distribution of adsorbed species between adsorbent and the solution at equilibrium are considered [42]. In this regards, various models such as Langmuir, Freundlich, and Redlich-Peterson isotherm models were used. Linear form of Langmuir equation is shown in Eq. (2) [43].

$$\frac{C_e}{q_e} = \frac{1}{q_m K_L} + \frac{C_e}{q_m} \tag{2}$$

C<sub>e</sub> is the Co<sup>2+</sup> concentration at equilibration (mg L<sup>-1</sup>), q<sub>e</sub> is the amount cation uptake by sorbent (mg g<sup>-1</sup>) at equilibrium, q<sub>m</sub> is maximal capacity (mg g<sup>-1</sup>), and K<sub>L</sub> is the Langmuir constant. By plotting C<sub>e</sub>/q<sub>e</sub> versus C<sub>e</sub> a straight line was obtained. The slope (1/q<sub>m</sub>), and the intercept (1/q<sub>m</sub> K<sub>L</sub>) of the line was used to determine the isotherm parameters.

The linear form of Freundlich isotherm is described by eq. (3) [44].

$$\ln q_e = \ln K_F + \frac{1}{n} \ln C_e \tag{3}$$

C<sub>e</sub> is Co<sup>2+</sup> concentration at equilibration (mg L<sup>-1</sup>), q<sub>e</sub> is adsorbed amount of cobalt at equilibration (mg g<sup>-1</sup>), n and K<sub>F</sub> are constants related respectively to intensity and capacity of adsorption. Plotting of lnq<sub>e</sub> against lnC<sub>e</sub> produced a straight line with slope and intercept equal to 1/n and K<sub>F</sub> respectively.

The linear form of Redlich-Peterson model is given in Eq. (4) [45].

$$\ln \left( A \frac{C_e}{q_e} - 1 \right) = g \ln C_e + \ln B \tag{4}$$

The for the By plotting of ln (A C<sub>e</sub>/q<sub>e</sub> - 1) versus ln C<sub>e</sub> a straight line was obtained. Its R<sup>2</sup> value, and was determined and the quantity of B and g were obtained from the slope and intercept of the plot. If g = 1, the isotherm is considered as the Langmuir isotherm [46].

Sips isotherm can be considered as a mixture of Langmuir and Freundlich, and its linear form is represented in Eq. (5) [47].

$$\frac{1}{q_e} = \frac{1}{Q_{max} K_s} \left( \frac{1}{C_e} \right)^{1/m} + \frac{1}{Q_{max}} \tag{5}$$

Q<sub>max</sub> is the maximal capacity (mgg<sup>-1</sup>), K<sub>s</sub> and m are the Sips equilibrium constant (L mg<sup>-1</sup>) and exponent constant respectively. The plot of 1/q<sub>e</sub> versus (1/C<sub>e</sub>)<sup>1/m</sup> gave a straight line and Q<sub>max</sub> and K<sub>s</sub> were determined from the slope and intercept of the plot. m is a characteristic dimensionless heterogeneity factor of Sips isotherm equation. If m is between 0 and 1, it represent heterogeneous system, while with m = 1, the sorption system is homogenous, and the Sips equation reduces to the Langmuir equation [48].

As indicated from the results of the studied isotherm (Table 6), the data were better described by the Redlich-Peterson isotherm.

### Error analysis

Since the R<sup>2</sup> of the linear analysis cannot alone evaluate the fitness of isotherms; therefore, the sum of squares of the errors (SSE) and the average relative errors (ARE) were used to evaluate fitness of data to the appropriate isotherm models (Eqs. 6 and 7) [49, 50].

$$SSE = \sum (q_c - q_e)^2 \tag{6}$$

$$ARE = \sum \frac{|(q_c - q_e)/q_e|}{n} \tag{7}$$

q<sub>c</sub> and q<sub>e</sub> are theoretical and experimental sorption capacity (mg g<sup>-1</sup>) respectively, and n is the number of data points. From the values of SSE and ARE (Table 6), it was concluded that ARE values were in the order of; Redlich-Peterson < Sips < Langmuir < Freundlich. Since the previous experiments showed that Redlich-Peterson equation reduced to the Langmuir equation, it can be concluded that the data was fitted to the Langmuir model.

**Table 9** Removal efficiency of cobalt ions from real samples by Co(II)-MIIP

| Sample    | Co <sup>2+</sup> Added (mg L <sup>-1</sup> ) | Co <sup>2+</sup> Found (mg L <sup>-1</sup> ) | R (%) | RSD % (n = 3) |
|-----------|--|--|-------|---------------|
| Solid     | 10   | 9.9  | 99.0  | 2.5           |
| Sea water | 10   | 9.9  | 99.0  | 2.8           |
| Sea well  | 10   | 10.1   | 101.0 | 2.7           |

**Table 10** Adsorption capacity of different sorbent for uptake of cobalt

| Adsorbents  | Adsorption capacity (mg g <sup>-1</sup> ) | Ref.       |
|---|---|------------|
| α-Fe <sub>2</sub> O <sub>3</sub>                                      | 20.50                                     | [57]       |
| Cone biomass  | 7.38                                      | [58]       |
| Modified palygorskite with 3-aminopropyl triethoxysilane              | 34.24                                     | [59]       |
| Dehydrated beet pulp carbon   | 58.00                                     | [60]       |
| MWCNT/IO  | 10.61                                     | [61]       |
| SiO <sub>2</sub> /Nb <sub>2</sub> O <sub>5</sub> /ZnO                 | 0.51                                      | [62]       |
| Ordered Micro and Mesoporous/SiO <sub>2</sub>                         | 8.43                                      | [63]       |
| Co(II)-imprinted 1-vinylimidazole                                     | 23.09                                     | [39]       |
| Co(II)-imprinted polyethyleneimine (PEI)                              | 39.26                                     | [40]       |
| Co(II)-imprinted 3-(2-aminoethylamino) propyltrimethoxysilane (AAPTS) | 35.21                                     | [41]       |
| Co(II)-MIIP   | 74.00                                     | This study |

## Kinetic of sorption process

To evaluate the kinetic of the process; Pseudo-first-order, and pseudo-second-order were implied [51]. The pseudo-first-order model is described by Eq. (8) [52].

$$\log(q_e - q_t) = \log q_e - \left( \frac{K_1}{2.303} \right) t \quad (8)$$

$K_1$  is rate constant (min<sup>-1</sup>),  $q_e$  and  $q_t$  are the sorbent capacity (mg g<sup>-1</sup>) respectively at equilibration and at  $t$  (min). Plotting of  $\log(q_e - q_t)$  versus  $t$  gave a straight line by which the kinetic parameters were calculated from the slope and intercept.

Linearized form of pseudo-second-order equation is represented in eq. (9) [53].

$$\frac{t}{q_t} = \frac{1}{K_2 q_e^2} + \left( \frac{1}{q_e} \right) t \quad (9)$$

$K_2$  is rate constant (min<sup>-1</sup>) (g/mg min),  $q_e$  and  $q_t$  are sorbent capacity (mg g<sup>-1</sup>) at equilibration and at  $t$  (min). By the slope and intercept of the line ( $t/q_t$  versus  $t$ ), the kinetic parameters were determined.

Kinetic parameters for the studied models is given in Table 7, and their linear plot are represented in Fig. 4S. The results revealed that the experimental data was described by pseudo-second-order model.

## Thermodynamic parameters

Thermodynamic parameters were measured by the following equations [52, 54]:

$$\ln K_d = \frac{\Delta S^\circ}{R} - \frac{\Delta H^\circ}{RT} \quad (10)$$

$$K_d = \frac{C_i - C_e}{C_e} \times \frac{V}{M} \quad (11)$$

$K_d$  is the distribution constant at equilibrium,  $R$  is the ideal gas constant,  $T$  (K) temperature,  $C_i$ , and  $C_e$  are initial and equilibrium concentrations respectively (mg L<sup>-1</sup>),  $V$  (mL) is the volume, and  $M$  (g) is mass of adsorbent. By plotting of  $\ln K_d$  versus  $1/T$  a straight line was obtained, and the enthalpy change ( $\Delta H^\circ$ ) and entropy change ( $\Delta S^\circ$ ) were respectively measured by the slope and intercept of the line (Fig. 6S). The Gibbs free energy change ( $\Delta G^\circ$ ) was then determined by following equation [55]:

$$\Delta G^\circ = \Delta H^\circ - T\Delta S^\circ \quad (12)$$

The positive values of  $\Delta G^\circ$ , and  $\Delta H^\circ$  (Table 8), indicated that the process was non-spontaneous, and endothermic respectively. The negative value of  $\Delta S^\circ$  showed that the randomness at the solid-solution surface was reduced during the adsorption process.

## Real sample analysis

The adsorption data showed that the selectivity of the sorbent for cobalt was high, therefore its capability in real samples (solid and liquid) with complicated matrix was evaluated. The solid sample was taken from an industrial zone (Asaluyeh region, south of Iran, Phase 9-SPD10), and digested according to the following procedure:

0.5 g of dried sample was powdered, 2 drops of HCl (0.1 M) and 7 mL of HF (48%) was added and the mixture heated until proper dryness. After adding 7 mL of acids (3:1 HCl:HNO<sub>3</sub>), it was for for 30 min, and then 5 mL HClO<sub>4</sub> was then added. The mixture was heated to dryness, and the solid

residue was dissolved in a few drop of HCl (1 M) and the diluted to 50 mL by deionized water [56].

Sea water and well water selected as liquid samples and were treated as follows:

To remove the organic compounds 3 mL of H<sub>2</sub>O<sub>2</sub> (30%) and 5 mL of HNO<sub>3</sub> was added, and the mixture was heated for 60 min at 80 °C. The mixture was filtered, and the solution was diluted to 100 mL by deionized water [56].

To each sample, the concentration of added nickel was adjusted to 10 mg L<sup>-1</sup>, and the sorption of cobalt was evaluated by Co(II)-MIIP at optimized conditions. The sorbent was removed, and the removal efficiency (R%) was calculated (Table 9). By the results it was concluded that adsorbent was capable to efficiently remove the studied cation from real samples. After optimizing the experimental conditions such as contact time, pH, sorbent dosage, and cation concentration, the adsorption capacity of 74 mg.g<sup>-1</sup> was obtained for Co(II)-MIIP which was superior to the other studied adsorbent used for removal of cobalt (Table 10).

## Conclusions

A functionalized magnetic cobalt ion-imprinted sorbent was prepared and characterized by different techniques. The sorption data revealed that under optimized conditions (adsorbent dose of 0.15 g, cobalt concentration of 1000 mgL<sup>-1</sup>, contact time of 5 min, and at pH = 8), the adsorption capacity was 74 mg g<sup>-1</sup>. Separation of the used sorbent was easily performed by external magnetic field, and was recovered by HNO<sub>3</sub> (1 M). The regenerated sample retained most of its initial capacity (85%) after seven regeneration cycles. The adsorption data was evaluated by Langmuir, Freundlich, Redlich-Peterson and Sips isotherms. Pseudo-first-order, and pseudo-second-order models were used to evaluate the kinetic of the process. The adsorption process was non-spontaneous and endothermic. The selectivity of the adsorbents in the presence of different cations and in real samples showed that it had high selectivity for the studied cation.

## Compliance with ethical standards

**Declaration on conflict of interest** There is no conflict of Interest.

## References

1. Yan X, Li QZ, Chai LY, Yang BT, Wang QW. Formation of a biological granular sludge – A facile and bioinspired proposal for improving sludge settling performance during heavy metal wastewater treatment. *Chemosphere*. 2014;113:36–41.
2. Repo E, Kumiawan TA, Warchol JK, Sillanpää MET. Removal of Co(II) and Ni(II) ions from contaminated water using silica gel functionalized with EDTA and/or DTPA as chelating agents. *J Hazard Mater*. 2009;171:1071–80.
3. Chai LY, Wang QW, Li QZ, Yang ZH, Wang YY. Enhanced removal of Hg(II) from acidic aqueous solution using thiol-functionalized biomass. *Water Sci Technol*. 2010;62:2157–65.
4. Wang QW, Qin WQ, Chai LY, Li QZ. Understanding the formation of colloidal mercury in acidic wastewater with high concentration of chloride ions by electrocapillary curves. *Environ Sci Pollut R*. 2014;21:3866–72.
5. Özkahraman B, Özbaş Z, Öztürk AB. Synthesis of ion-imprinted alginate based beads: selective adsorption behavior of nickel (II) ions. *J Polym Environ*. 2018;26(11):4303–10.
6. Pourjavid MR, Arabieh M, Yousefi SR, Jamali MR, Rezaee M, Haji Hosseini M, et al. Study on column SPE with synthesized graphene oxide and FAAS for determination of trace amount of Co(II) and Ni(II) ions in real sample. *Mater Sci Eng*. 2015;47:114–22.
7. Rafati L, Nabizadeh R, Mahvi AH, Dehghani MH. Removal of phosphate from aqueous solutions by iron nano-particle resin Lewatit (FO36). *Korean J Chem Eng*. 2012;29(4):473–7.
8. Mauchauffée S, Meux E. Use of sodium decanoate for selective precipitation of metals contained in industrial wastewater. *Chemosphere*. 2007;69:763–8.
9. Rengaraj S, Yeon KH, Kang SY, Lee JU, Kim KW, Moon SH. Studies on adsorptive removal of co(II), Cr(III) and Ni(II) by IRN77 cation-exchange resin. *J Hazard Mater*. 2002;B92:185–98.
10. El Samrani AG, Lartiges BS, Villieras F. Chemical coagulation of combined sewer overflow: heavy metal removal and treatment optimization. *Water Res*. 2008;42:951–60.
11. Rengaraj S, Moon SH. Kinetics of adsorption of Co(II) removal from water and wastewater by ion-exchange resins. *Water Res*. 2002;36:1783–93.
12. Mohsen-Nia M, Montazeri P, Modarress H. Removal of Cu<sup>2+</sup> and Ni<sup>2+</sup> from wastewater with a chelating agent and reverse osmosis processes. *Desalination*. 2007;217:276–81.
13. Kumiawan TA, Chan GYS, Lo WH, Babel S. Comparisons of low-cost adsorbents for treating wastewaters laden with heavy metals. *Sci Total Environ*. 2006;366:409–26.
14. Gallego-Gallegos M, Muñoz-Olivas R, Martín-Esteban A, Cámara C. Synthesis and evaluation of molecularly imprinted polymers for organotin compounds: A screening method for tributyltin detection in seawater. *Anal Chim Acta*. 2005;531:33–9.
15. Ramstrom O, Ansell R. Molecular imprinting technology: challenges and prospects for the future. *J Chirality*. 1998;10:195–209.
16. Saraji M, Yousefi H. Selective solid-phase extraction of Ni(II) by an ion-imprinted polymer from water samples. *J Hazard Mater*. 2009;167:1152–7.
17. Rao TP, Kala R, Daniel S. Metal ion-imprinted polymers—novel materials for selective recognition of inorganics. *Anal Chim Acta*. 2001;578:105–16.
18. Burham N. Separation and preconcentration system for lead and cadmium determination in natural samples using 2-aminoacetylthiophenol modified polyurethane foam. *Desalination*. 2009;249:1199–205.
19. Rivera-Jiménez SM, Méndez-González S, Hernández-Maldonado A. Metal (M = Co<sup>2+</sup>, Ni<sup>2+</sup>, and Cu<sup>2+</sup>) grafted mesoporous SBA-15: effect of transition metal incorporation and pH conditions on the adsorption of naproxen from water. *Microporous Mesoporous Mater*. 2010;132:470–9.
20. Rafati L, Ehrampoush MH, Rafati AA, Mokhtari M, Mahvi AH. Nanocomposite adsorbent based on β-cyclodextrin-PVP-clay for the removal of naproxen from aqueous solution: fixed-bed column and modeling studies. *Desalin Water Treat*. 2018;132:63–74.
21. Zhang JN, Ma Z, Jiao J, Yin HF, Yan WF, Hagaman EW, et al. Layer-by-layer grafting of titanium phosphate onto Mesoporous

- silica SBA-15 surfaces: synthesis, characterization, and applications. *Langmuir*. 2009;25:12541–9.
22. Moradi Kalhor M, Rafati AA, Rafati L, Rafati AA. Synthesis, characterization and adsorption studies of amino functionalized silica nano hollow sphere as an efficient adsorbent for removal of imidacloprid pesticide. *J Mol Liq*. 2018;266:453–9.
  23. Wang J, Zheng S, Shao Y, Liu J, Xu Z, Zhu D. Amino-functionalized  $\text{Fe}_3\text{O}_4@/\text{SiO}_2$  core-shell magnetic nanomaterial as a novel adsorbent for aqueous heavy metals removal. *J Colloid Interface Sci*. 2010;349:293–9.
  24. Wang S, Wang KA, Dai C, Shi H, Li J. Adsorption of  $\text{Pb}^{2+}$  on amino-functionalized core-shell magnetic mesoporous SBA-15 silica composite. *Chem Eng J*. 2015;262:897–903.
  25. Pérez-Quintanilla D, del Hierro I, Fajardo M, Sierra I. Microporous Mesoporous Mater. 2006;89:58–68.
  26. Tadjarodi A, Jalalat V, Zare-Dorabei R. Synthesis and characterization of functionalized SBA-15 Mesoporous Silica by N, N'-Bis(salicylidene)ethylenediamine Schiff-Base. *J Nanotech Struct*. 2013;3:477–82.
  27. Faisal M, Ismail AA, Harraz FA, Bouzid H, Al-Sayari S, Al-Hajry A. Mesoporous  $\text{TiO}_2$  based optical sensor for highly sensitive and selective detection and preconcentration of Bi(III) ions. *Chem Eng J*. 2014;243:509–16.
  28. Chmelka BF, Stucky GD, Zhao DY, Feng JL, Huo QS, Melosh N, et al. Triblock copolymer syntheses of mesoporous silica with periodic 50 to 300 angstrom pores. *Sci*. 1998;279:548–52.
  29. Jiang Y, Liu Y, Liu Z, Qiu J, Meng M, Ni L, et al. Selective Ce(III) ion-imprinted polymer grafted on  $\text{Fe}_3\text{O}_4$  nanoparticles supported by SBA-15 mesopores microreactor via surface-initiated RAFT polymerization. *Microporous Mesoporous Mater*. 2016;234:176–85.
  30. Kang YS, Zhao S, Lee DK, Kim Ch W, Cha HG, Kim YH. Synthesis of magnetic nanoparticles of  $\text{Fe}_3\text{O}_4$  and  $\text{CoFe}_2\text{O}_4$  and their surface modification by surfactant adsorption. *Bull Korean Chem Soc*. 2006;27:237–42.
  31. Kazeminezhad I, Mosivand S. Phase transition of Electrooxidized  $\text{Fe}_3\text{O}_4$  to  $\gamma$  and  $\alpha$ - $\text{Fe}_2\text{O}_3$  nanoparticles using sintering treatment. *Acta Phys Pol*. 2014;A125:1210–4.
  32. Bagheri A, Behbahani M, Taghizadeh M, Salarian M, Sadeghi O, Adlnasab L, et al. Synthesis and characterization of nano structure lead (II) ion-imprinted polymer as a new sorbent for selective extraction and preconcentration of ultra trace amounts of lead ions from vegetables, rice, and fish samples. *Food Chem*. 2013;138(2–3):2050–6.
  33. Sayar O, Akbarzadeh Torbati N, Saravani H, Mehrani K, Behbahani A, Moghadam ZH. A novel magnetic ion imprinted polymer for selective adsorption of trace amounts of lead(II) ions in environment samples. *J Ind Eng Chem*. 2014;20(5):2657–62.
  34. Fayazi M, Taher MA, Afzali D, Mostafavi A, Ghanei-Motlagh M. Synthesis and application of novel ion-imprinted polymer coated magnetic multi-walled carbon nanotubes for selective solid phase extraction of lead(II) ions. *Mater Sci Eng*. 2016;C(60):365–73.
  35. Zhang H, Dou Q, Jin X, Sun D, Wang D, Yang T. Magnetic Pb(II) Ion-imprinted polymer prepared by surface imprinting technique and its adsorption properties. *Sep Sci Technol*. 2015;50:901–10.
  36. Xu X, Wang M, Wu Q, Xu Z, Tian X. Synthesis and application of novel magnetic ion-imprinted polymers for selective solid phase extraction of Cadmium (II). *Polym*. 2017;(9):360–70.
  37. Xi Y, Luo Y, Luo J, Luo X. Removal of Cadmium(II) from wastewater using novel cadmium ion-imprinted polymers. *J Chem Eng Data*. 2015;60(11):3253–326.
  38. Luo X, Luo S, Zhan Y, Shu H, Huang Y, Tu X. Novel Cu (II) magnetic ion imprinted materials prepared by surface imprinted technique combined with a sol-gel process. *J Hazard Mater*. 2011;192:949–55.
  39. Kang R, Qiu L, Fang L, Yu R, Chen Y, Lu X, et al. A novel magnetic and hydrophilic ion-imprinted polymer as a selective sorbent for the removal of cobalt ions from industrial wastewater. *J Environ Chem Eng*. 2016;(4):2268–77.
  40. Yan L, Zhancha L, Jiangdong D, Jie G, Jimin X, Yongsheng Y. Selective adsorption of Co(II) by Mesoporous Silica SBA-15-supported surface ion imprinted polymer: kinetics, isotherms, and thermodynamics studies. *Chin J Chem*. 2011;29:387–98.
  41. Khoddami N, Shemirani F. A new magnetic ion-imprinted polymer as a highly selective sorbent for determination of cobalt in biological and environmental samples. *Talanta*. 2016;146:244–52.
  42. Rafati L, Ehrampoush MH, Rafati AA, Mokhtari M, Mahvi AH. Removal of ibuprofen from aqueous solution by functionalized strong nano-clay composite adsorbent: kinetic and equilibrium isotherm studies. *Int J Environ Sci Technol*. 2018;15:513–24.
  43. Langmuir. The constitution and fundamental properties of solids and liquids. *J Am Chem Soc*. 1916;38(5):2221–95.
  44. Freundlich HMF. Over the adsorption in solution. *Z Phys Chem*. 1906;57A(5):385–470.
  45. Redlich O, Peterson DL. A useful adsorption isotherm. *J Phys Chem*. 1959;63(5):1024.
  46. Juang RS, Wu FC, Tseng RL. Adsorption isotherms of phenolic compounds from aqueous solutions onto activated carbon fibers. *J Chem Eng Data*. 1996;41(3):487–92.
  47. Yang RT. Adsorbents: fundamentals and applications. New Jersey: Wiley; 2003.
  48. Allen SJ, Mckay G, Porter JF. Adsorption isotherm models for basic dye adsorption by peat in single and binary component systems. *J Colloid Interface Sci*. 2004;280(2):322–33.
  49. Foo KY, Hameed BH. Insights into the modeling of adsorption isotherm systems. *Chem Eng J*. 2010;156(1):2–10.
  50. Rafati L, Ehrampoush MH, Rafati AA, Mokhtari M, Mahvi AH. Modeling of adsorption kinetic and equilibrium isotherms of naproxen onto functionalized nano-clay composite adsorbent. *J Mol Liq*. 2016;224:832–41.
  51. Kamranifar M, Khodadadi M, Samiei V, Dehdashti B, Noori Sepehr M, Rafati L, et al. Comparison the removal of reactive red 195 dye using powder and ash of barberry stem as a low cost adsorbent from aqueous solutions: isotherm and kinetic study. *J Mol Liq*. 2018;255:572–7.
  52. Gunay A, Arslankaya E, Tosun I. Lead removal from aqueous solution by natural and pretreated clinoptilolite: Adsorption equilibrium and kinetics. *J Hazard Mater*. 2007;146:362–71.
  53. Martins RJE, Vilar VJP, Boaventura RAR. Kinetic modelling of cadmium and lead removal by aquatic mosses. *Braz J Chem Eng*. 2014;31(1):229–42.
  54. Bektas N, Agim BA, Kara S. Kinetic and equilibrium studies in removing lead ions from aqueous solutions by natural sepiolite. *J Hazard Mater*. 2004;B(112):115–22.
  55. Fan T, Liu Y, Feng B, Zeng G, Yang C, Zhou M, et al. Biosorption of cadmium(II), zinc(II) and lead(II) by *Penicillium simplicissimum*: Isotherms, kinetics and thermodynamics. *J Hazard Mater*. 2008;160:655–61.
  56. Huang Ch HB. Silica-coated magnetic nanoparticles modified with  $\gamma$ - mercaptopropyltrimethoxysilane for fast and selective solid phase extraction of trace amounts of Cd, Cu, Hg, and Pb in environmental and biological samples prior to their determination by inductively coupled plasma mass spectrometry. *Spectrochim. Acta*. 2008;63:437–44.
  57. Nassar MY, Ahmed IS, Mohamed TY, Khatab M. A controlled, templatefree, and hydrothermal synthesis route to sphere-like [small alpha]- $\text{Fe}_2\text{O}_3$  nanostructures for textile dye removal. *RSC Adv*. 2016;6:20001–13.
  58. Aksakal O, Ucin H. Equilibrium, kinetic and thermodynamic studies of the biosorption of textile dye (reactive red 195) onto *Pinus sylvestris* L. *J Hazard Mater*. 2010;181:666–72.

59. Xue A, Zhou S, Zhao Y, Lu X, Han P. Adsorption of reactive dyes from aqueous solution by silylated palygorskite. *Appl Clay Sci.* 2010;48:638–40.
60. Dursun AY, Tepe O. Removal of Chemazol reactive red 195 from aqueous solution by dehydrated beet pulp carbon. *J Hazard Mater.* 2011;194:303–11.
61. Ibezim-Ezeani MU, Okoye FA, Akaranta O. Studies on the ion exchange properties of modified and unmodified orange mesocarp extract in aqueous solution. *Int Arch Appl Sci Technol.* 2010;1:33–40.
62. Ramila A, Munoz B, Pariente JP, Regí MV. Mesoporous MCM-41 as drug host system. *J Sol Gel Sci Technol.* 2003;26:1199–202.
63. Andersson J, Rosenholm J, Areva S, Linden M. Influences of material characteristics on ibuprofen drug loading and release profiles from ordered micro- and mesoporous silica matrices. *Chem Mater.* 2004;16:4160–7.

**Publisher's note** Springer Nature remains neutral with regard to jurisdictional claims in published maps and institutional affiliations.